# A novel cell-cycle-regulated interaction of the Bloom syndrome helicase BLM with Mcm6 controls replication-linked processes

**Vivek M. Shastri[1,†], Veena Subramanian[1,†] and Kristina H. Schmidt** [ORCID][1,2,*]

[1]Department of Cell Biology, Microbiology and Molecular Biology, University of South Florida, Tampa, FL 33620, USA and [2]Cancer Biology and Evolution Program, H. Lee Moffitt Cancer Center and Research Institute, Tampa, FL 33612, USA

## ABSTRACT

**The Bloom syndrome DNA helicase BLM contributes to chromosome stability through its roles in double-strand break repair by homologous recombination and DNA replication fork restart during the replication stress response. Loss of BLM activity leads to Bloom syndrome, which is characterized by extraordinary cancer risk and small stature. Here, we have analyzed the composition of the BLM complex during unperturbed S-phase and identified a direct physical interaction with the Mcm6 subunit of the minichromosome maintenance (MCM) complex. Using distinct binding sites, BLM interacts with the N-terminal domain of Mcm6 in G1 phase and switches to the C-terminal Cdt1-binding domain of Mcm6 in S-phase, with a third site playing a role for Mcm6 binding after DNA damage. Disruption of Mcm6-binding to BLM in S-phase leads to supra-normal DNA replication speed in unperturbed cells, and the helicase activity of BLM is required for this increased replication speed. Upon disruption of BLM/Mcm6 interaction, repair of replication-dependent DNA double-strand breaks is delayed and cells become hypersensitive to DNA damage and replication stress. Our findings reveal that BLM not only plays a role in the response to DNA damage and replication stress, but that its physical interaction with Mcm6 is required in unperturbed cells, most notably in S-phase as a negative regulator of replication speed.**

## INTRODUCTION

Genomic instability is a hallmark of disorders in which DNA repair genes are dysfunctional (1). The prevention of genomic instability depends on multiple pathways ensuring timely progression of replication and appropriate response to DNA damage. The tumor suppressor gene *BLM* encodes a 3′–5′ DNA helicase of the conserved RecQ DNA helicase family, which has been implicated in key roles during homologous recombination (HR) and DNA repair to maintain genome stability (2–4). Null mutations in *BLM* cause Bloom syndrome (BS), an autosomal recessive disorder characterized by short stature, an extreme predisposition to a wide range of cancers from an early age and, at the cellular level, elevated levels of sister chromatid exchanges (SCEs), chromosome aberrations and hypersensitivity to DNA-damaging agents (5–7). The best-understood function of BLM is the dissolution of double Holliday junctions during HR-mediated DNA double strand break (DSB) repair where BLM acts in a complex with TopoIIIα, Rmi1 and Rmi2 to yield noncrossover products (8). BLM also controls early steps of HR by contributing to the long-range processing of DSB ends into single-stranded 3′ overhangs for strand invasion and through its ability to reverse the strand invasion step (9).

BLM helicase function is also required for efficient restart of stalled replication forks in the presence of replication stress. In the absence of BLM, cells exposed to replication-stress-inducing agents like hydroxyurea (HU) display compromised fork reactivation and delayed cell division (10). Of all stalled replication forks, fewer than 40% restart in BS cells (11). Studies have shown BLM localization to stalled replication forks that develop into DSBs (12). Chromatin recruitment of DNA-damage-response factors like BRCA1, 53BP1 and the MRN complex to stalled replication forks is delayed in BS cells, leading to BLM being associated with a role in their recruitment and facilitating fork protection (12,13). These observations establish BLM as an important factor in the replication stress response.

BLM's function in recombinational repair has been proposed as a plausible mechanism by which it promotes fork restart upon replication stress induction. *In vitro* analyses have shown that BLM can promote regression of model

replication forks ([14](#)) and the high level of SCEs in BS cells has been viewed as possible evidence of illegitimate mitotic recombination products when collapsed replication forks undergo DSB repair ([15,16](#)).

*In vitro*, BLM has been shown to bind and unwind G-quadruplex (G4) structures ([17–19](#)). *In vivo*, G4s are stable secondary DNA structures that impede replication fork progression, especially at telomeres ([20](#)) and there is emerging evidence of a direct role of BLM in G4 unwinding *in vivo*, including slow moving replication forks originating within the G4-rich telomeric sequences in BS cells ([21,22](#)). Further underscoring BLM's specificity for a variety of non-canonical DNA substrates, BLM can also unwind model DNA:RNA hybrids and R-loops *in vitro*, which can cause replication fork stalling ([23](#)). Observations of R-loop accumulation causing DNA damage in BS cells and BLM/R-loop proximity *in vivo* seem to imply BLM involvement in maintaining replisome stability at sites of collision with R-loops ([24](#)).

The six-subunit minichromosome maintenance (MCM) complex is an essential component of the eukaryotic replisome and functions in DNA replication initiation and elongation. It is the catalytic subunit of the major replicative helicase complex and is loaded onto DNA replication origins in a stepwise manner by the licensing factor Cdt1 ([25](#)). An excessive amount of the MCM complex is loaded onto replication origins, but not all fire in the following S-phase. These so-called dormant origins fire under low levels of endogenous replication stress and may prevent DSBs forming from stalled DNA replication forks ([26](#)). The MCM complex also serves as an important component of the replication checkpoint and is an effector of the ATR–FANCD2–FANCI pathway activated in response to replication stress ([27,28](#)). However, additional mechanisms that facilitate replication fork movement through challenging loci, including those containing non-canonical DNA structures, are likely to be required ([29](#)).

To gain insight into the importance of the BLM helicase during the unperturbed cell cycle and better understand the mechanism by which BLM contributes to stable genome duplication, we determined the composition of the BLM complex in unperturbed mid-S-phase cells when BLM levels are highest. We identified the MCM subunit Mcm6 as a novel BLM interactor and show that BLM uses distinct binding sites to associate with Mcm6 in G1, during unperturbed S-phase, and during the DNA-damage response. Our findings reveal that BLM helicase activity is capable of accelerating replication speed in unperturbed cells and that the physical association between BLM and Mcm6 restricts this activity and is essential for maintaining normal replication fork speed. The BLM/Mcm6 interaction also contributes to efficient repair of replication-dependent DNA double-strand breaks and to the replication stress response.

## MATERIALS AND METHODS

### Human cell lines used in this study

GM00637 is a SV40-transformed human skin fibroblast cell line and was obtained from the NIGMS Human Genetic Cell Repository at the Coriell Institute. The bi-allelic *BLM* knockout cell line KSVS1452 (*BLM$^{KO}$*) was derived from GM00637 (WT) by bi-allelic disruption of *BLM* exon 8 by CRISPR/Cas9 ([30](#)). KSVS1454 (*BLM$^{KO/+}$*) was derived from KSVS1452 (*BLM$^{KO}$*) by stable transfection with *BLM* cDNA and expresses wildtype BLM at a similar level to the BLM wildtype cell line GM00637 ([30](#)). KSVS1452-derived cell lines stably expressing mutant *BLM* cDNAs that were generated for this study are listed in Supplemental Table S1.

### Transfections with siRNAs and plasmid DNA

For transient transfection with plasmid DNA, KSVS1452 (*BLM$^{KO}$*) cells were seeded in 6-well plates and, at a confluency of 70–80%, transfected with plasmid DNA using Lipofectamine 3000 (Invitrogen) in Opti-MEM medium according to the manufacturer's protocol. After 72 h, BLM expression was evaluated by western blotting and cells were used for downstream applications. For transfection with siRNAs, multiple pre-designed siRNAs per target gene as well as scrambled control siRNA were obtained from Invitrogen (Ambion InVivo siRNAs) and Bioneer (AccuTarget siRNAs). GM00637 (*BLM$^{+/+}$*) cells were transfected at 70–80% confluency in six-well plates with 50 nM of siRNA using Lipofectamine RNAiMAX (Invitrogen) in Opti-MEM medium following the manufacturer's protocol. Downregulation of target genes was analyzed by Western blotting and immunofluorescence microscopy 48 hours after transfection.

### Double-thymidine block and nocodazole block

Cells in G1 phase were obtained as previously described ([31](#)). Briefly, cells were cultured in serum-free media for 22 hours, released into media with 10% FBS for 2 h, treated with 50 ng/mL nocodazole for 16 hours and released into G1 phase over several hours. For synchronization in S phase, cells were arrested at G1/S by double-thymidine block and released into S-phase for three hours. To induce DNA double-strand breaks, cells were released into S phase for 3 h, treated with 1 μM camptothecin (CPT) for 1 h and released into CPT-free media.

### Co-immunoprecipitation

Nuclear extracts were prepared from exponentially growing cells as previously described ([32](#)). Cells were lysed (20 mM Tris pH 7.4, 10 mM KCl, 1 μM EDTA, 0.2% NP40, 50% glycerol, 0.6 mM βME, 1 mM PMSF and protease inhibitor cocktail [Pierce]) for 2 min on ice to isolate nuclei. Nuclei were lysed in 20 mM Tris pH 7.4, 10 mM KCl, 0.4 M NaCl, 1 μM EDTA, 50% glycerol, 0.6 mM βME, 1 mM PMSF, and protease inhibitor cocktail supplemented with 25 U/ml benzonase (Novagen). Nuclear lysate was diluted, precleared and incubated overnight at 4°C with either anti-BLM A300-110A (Bethyl), anti-MCM6 H8 (SCBT) or IgG crosslinked to Protein G Agarose (Pierce). Alternatively, chromatin-bound fractions were prepared for co-immunoprecipitation as described below. One milligram of nuclear or chromatin fractions were precleared with 30 μl Protein G agarose beads (Pierce) at 4°C for 1 h. The precleared lysates were incubated overnight at 4°C with end-over-end mixing with either anti-BLM A300-110A (4 μg; Bethyl), anti-MCM6 H8 (4 μg; SCBT), or

non-specific IgG crosslinked to Protein G Agarose beads (Pierce), and washed extensively prior to elution with 50 $\mu$l 2× Laemmli sample buffer. For LC–MS/MS, complexes were eluted in 50 $\mu$l 0.2 M glycine, pH 2.6 and immediately neutralized with 50 $\mu$l Tris, pH 8.0. To analyze BLM complex composition, co-immunoprecipitation eluates were prepared for mass spectrometry by FASP (Expedeon), followed by trypsin digestion (Promega), desalting and concentration, resuspended in 0.1% formic acid and analyzed on a Q Exactive Plus (Thermo). LC–MS/MS data was analyzed using MaxQuant (33). Spectra were compared against the UniProt reference proteome data set for *Homo sapiens* (Proteome ID: UP000005640). Data sets were sorted to only include entries without identified peptides in eluates from IgG immunoprecipitations and in KSVS1452 (*BLM^{KO}*). The mass spectrometry proteomics data have been deposited to the ProteomeXchange Consortium (http://proteomecentral.proteomexchange.org) via the PRIDE partner repository (34) with the dataset identifier PXD018823. For co-immunoprecipitations using recombinant BLM and Mcm6, full length human Mcm6 purified from wheat germ was obtained from Abcam. Full-length human BLM with a C-terminal His$_6$-tag was overexpressed in budding yeast from plasmid pJK1 (2) and purified over HisTrapHP, hydroxyapatite and MonoS columns on an ÄKTA FPLC as previously described (35).

### Extraction of chromatin-bound proteins by biochemical fractionation

Cells were incubated in hypotonic lysis buffer (10 mM HEPES pH 7.9, 10 mM KCl, 1.5 mM, MgCl$_2$, 0.34 M sucrose, 10% glycerol, 1 mM DTT, 1 mM PMSF, and 0.04% Triton X-100) on ice for 10 min and soluble proteins were separated by centrifugation at $2000 \times g$. The chromatin-enriched pellet was washed with low stringency buffer (3 mM EDTA, 0.2 mM EGTA, 1 mM DTT) and centrifuged at $1600 \times g$. Chromatin-bound proteins were extracted by incubating in ice cold RIPA buffer (50 mM Tris–HCl, pH 7.4, 1% NP-40, 0.1% sodium deoxycholate, 150 mM NaCl, 1 mM EDTA) followed by centrifugation at $16\,000 \times g$ (36,37).

### Immunofluorescence microscopy

Cells were cultured on glass coverslips for at least 24 h before cell cycle synchronization. For plasmid-borne protein expression, synchronization was initiated 24 h post-transfection. Cells at indicated time points in G1 and S phase were washed with PBS and extracted in ice cold extraction buffer (10 mM PIPES, pH 6.8, 300 mM sucrose, 100 mM NaCl, 1 mM MgCl$_2$, 1 mM EGTA, 1 mM DTT, 0.05% Triton X-100 and protease inhibitor cocktail). Cells were fixed using 4% paraformaldehyde for 15 min and permeabilized in 0.25% Triton-X-100 in PBS for 15 min at RT. After blocking in 1% BSA in PBS + 0.1% Tween-20 for 30 min, cells were incubated overnight at 4°C with primary antibodies: anti-BLM (C-18) (SCBT), anti-MCM6 (H-8) (SCBT), anti-Mcm2 (E-8) (SCBT), anti-Mcm7 (141.2) (SCBT), anti-Cdt1 (EPR17891) (Abcam),

anti-53BP1 (E-10) (SCBT) or anti-PML (PG-M3) (SCBT) followed by incubation with Alexa Fluor labeled secondary antibodies. Specificity of BLM immunostaining with anti-BLM (SCBT) and anti-BLM (Abcam) was verified in *BLM^{KO}* cells. Images were acquired with a PerkinElmer UltraVIEW ERS spinning disc confocal imager equipped with a 63×/1.4 Oil DIC Plan-Apochromat objective, or with a Nikon C2 Confocal Scanner with a 60×/1.4 Oil DIC CFI Plan Apochromat Lambda objective.

### Mammalian two-hybrid analysis

Full length human *BLM* and *MCM6* cDNAs were cloned into the pVP16 and pM vectors, respectively (Clontech). Fragments and point mutants in pVP16-BLM and pM-MCM6 were verified by DNA sequencing. SEAP activity expressed from a reporter vector was determined 72 h post-transfection using the Great EscAPe SEAP Fluorescence Detection Kit (Clontech). All co-transfections were performed in triplicate.

### DNA fiber labeling and analysis

DNA replication rates were measured by labeling DNA fibers based on a protocol described earlier (38). Cells at 50–70% confluency were labeled with 20 $\mu$M CldU (Sigma) for 30 min, followed by 100 $\mu$M IdU (Sigma) for 30 min. DNA fibers from lysed cells were allowed to stretch and airdry for 40 min at room temperature. After fixing, DNA was denatured and blocked with 10% goat-serum/PBS-T. Slides were incubated with rat anti-CldU (Abcam) and mouse anti-IdU (Becton Dickinson), washed, incubated with goat anti-rat IgG Alexa Fluor 594 (Invitrogen) and goat anti-mouse Alexa Fluor 488 Plus (Invitrogen) and imaged on a Keyence BZ-X fluorescence microscope with a CFI Achromat 60×/0.8 objective. Fibers showing a red label extended by a green label were analyzed for each cell line using ImageJ and the length of the green label was measured. DNA fiber analysis was performed at least twice for every cell line and a representative analysis of a minimum of 100 fibers is shown.

### Clonogenic assay

1000 cells/well were seeded 24 h post-transfection, released into media supplemented with pyridostatin (ApexBio) or hydroxyurea (US Biological) 24 h after seeding and incubated for 3 weeks. Cells were washed, fixed and stained with 0.01% crystal violet. Colonies containing more than 50 cells were scored as survivors. Assays were performed in triplicate.

## RESULTS

### BLM forms a complex with Mcm6 in G1 and S-phase

To test the possibility that BLM plays a role during unperturbed DNA replication we sought to determine the composition of the BLM complex in mid-S-phase when BLM expression peaks in unperturbed cells (Figure 1A). We
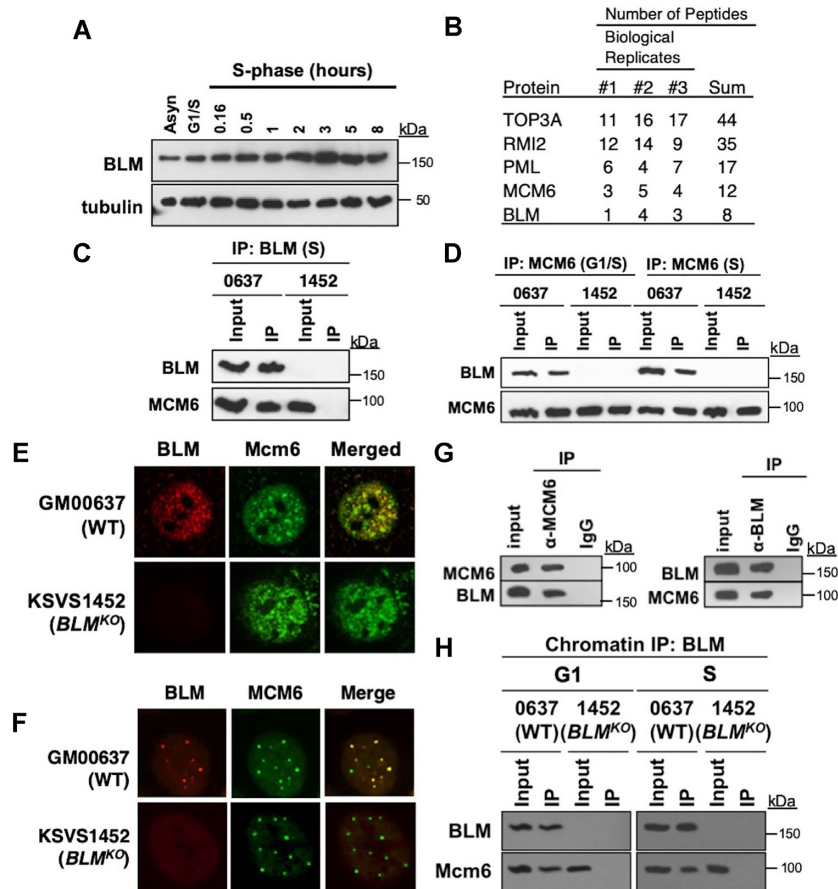
**Figure 1.** BLM binds to Mcm6 in unperturbed G1 and S-phase. (**A**) $BLM^{+/+}$(GM00637) cells were arrested at the G1/S boundary by double thymidine block, released into S-phase and BLM expression levels analyzed by Western blot. (**B**) Co-immunoprecipitations of endogenous BLM were performed in triplicate on nuclear extracts from $BLM^{+/+}$(GM00637) cells in mid-S phase and peptides were identified by mass spectrometry. The same analysis in triplicate for the isogenic *BLM* knockout cell line KSVS1452 ($BLM^{KO}$) yielded zero hits for the listed proteins. Cell lines GM00637 and KSVS1452 are an isogenic pair of a $BLM^{+/+}$ and a CRISPR-mediated $BLM^{KO}$ cell line, respectively. (**C, D**) Reciprocal co-immunoprecipitations of endogenous BLM and Mcm6 were performed on nuclear extracts of $BLM^{+/+}$ (GM00637) cells at G1/S and in mid-S phase. (**E**) Laser-scanning confocal microscopy images of fixed GM00637 ($BLM^{+/+}$) cells and KSVS1452 ($BLM^{KO}$) cells showing immunostaining of endogenous BLM [anti-BLM C18 (SCBT)] and Mcm6 [anti-Mcm6 H8 (SCBT) (**F**) Same cover slips of immunostained GM00637 ($BLM^{+/+}$) and KSVS1452 ($BLM^{KO}$) cells imaged in *(E)* were imaged on a Perkin Elmer ERS spinning disk confocal system visualizing large replication foci. For a different BLM and Mcm6 antibody combination and additional Mcm6 antibody verification, see Supplemental Figure S2A–C. (**G**) Reciprocal co-immunoprecipitations of recombinant human BLM (from yeast) and Mcm6 (from wheat germ). (**H**) $BLM^{+/+}$ cells (GM00637) were serum-starved for 16 hours, released for 2 h, blocked at G2/M with nocodazole, released for 6 h (mid-G1) and chromatin-bound proteins extracted by biochemical fractionation. Endogenous BLM was co-immunoprecipitated from the chromatin-bound protein fractions isolated in mid-G1 and in mid-S-phase.

synchronized GM00637 cells ($BLM^{+/+}$) at the G1/S boundary by double thymidine block, released them into S phase for 3 h, immunoprecipitated endogenous BLM from nuclear extracts and identified co-immunoprecipitates by mass spectrometry. Across three replicates, we identified the known BLM interactors Topo IIIα (39), Rmi2 (40), and PML (41), validating our approach (Figure 1B). We also identified Mcm6, a subunit of the minichromosome maintenance complex (MCM) (Figure 1B). We verified the novel interaction between BLM and Mcm6 by reciprocal co-immunoprecipitation using endogenous BLM and Mcm6 from nuclear extracts of synchronized GM00637 ($BLM^{+/+}$) cells (Figure 1C and D). The BLM/Mcm6 interaction was present not only in S-phase but also at the G1/S boundary (Figure 1D) whereas we did not detect the interaction in G2/M (Supplemental Figure S1). As expected, the interaction was absent from the isogenic KSVS1452 ($BLM^{KO}$)

cell line (Figure 1C and D) in which we prevented BLM expression by disrupting exon 8 in both *BLM* alleles using CRISPR/Cas9 (30). Reciprocal co-immunoprecipitations using recombinant human BLM (expressed in yeast) and human Mcm6 (translated in wheat germ extract) showed that the interaction between BLM and Mcm6 is direct (Figure 1G). All co-immunoprecipitations were performed in the presence of benzonase, indicating that the BLM/Mcm6 interaction is not mediated by DNA. Using antibodies directed against endogenous BLM and Mcm6, we observed that both proteins form an abundance of foci of variable sizes throughout the nucleus that largely overlap in S-phase (Pearson correlation coefficient: $0.65 \pm 0.038$) (Figure 1E). Visualizing the largest foci, BLM colocalized with Mcm6 (Figure 1F), which we further verified by using different primary BLM and Mcm6 antibodies (Supplemental Figure S2A). We further verified the Mcm6 antibody in West-

ern blots and immunofluorescence microscopy by knocking down Mcm6 expression using two different siRNAs (Supplemental Figure S2B and C).

Most of BLM and Mcm6 colocalized throughout S-phase (Supplemental Figure S2D). BLM is also known to localize to PML bodies [39]; however, BLM foci that colocalized with Mcm6 foci never colocalized with PML (Supplemental Figure S2E). Since MCM and BLM perform their functions on DNA, we also extracted chromatin-fractions from BLM-proficient cells (GM00637) and performed co-immunoprecipitions, showing that chromatin-bound BLM and Mcm6 interact in G1 and in S-phase (Figure 1H).

### BLM binds to the N-terminal domain of Mcm6 via a pseudo-PIP-box

Mcm2-7, the subunits of the MCM complex, can be divided into an N-terminal domain, which contains the oligonucleotide-binding (OB) domain, and a C-terminal domain, which contains the conserved ATPase core and an extension defined by a winged-helix (WH) domain [42]. In human Mcm6, the N-terminal domain spans residues 1–325 and the C-terminal domain spans residues 326–821. Using a mammalian two-hybrid assay, we determined that BLM interacts with both of these Mcm6 domains (Figure 2A, B). Dividing BLM into its two major domains—the disordered N-terminal tail (residues 1–647) and the C-terminal helicase domain (residues 648–1417) (Supplemental Figure S3A) – we determined that both, the N- and the C-terminal Mcm6 segments, interacted with BLM's disordered tail (residues 1–647). We narrowed down the binding site for the N-terminal segment of Mcm6 to residues 80–120 of BLM (Figure 2A, see also Supplemental Figure S3B–D). This disordered region in BLM contains the sequence $^{83}$QQRVKDFF$^{90}$ (Figure 2C), reminiscent of a PCNA-interacting-protein (PIP) box [43]. Mutating this sequence to $^{83}$AQRAKDAA$^{90}$ (hereafter referred to as the blm-QVFF mutation) significantly reduced the two-hybrid interaction between Mcm6 and BLM (Figure 2E). Alanine substitution of other hydrophobic residues in the 80–120 region of BLM, such as L107/L108 or F111, did not have a significant effect on Mcm6 binding (Supplemental Figure S3E).

Prompted by the resemblance of the Mcm6-binding site to a PIP-box we tested by co-immunoprecipitation if the $^{83}$QQRVKDFF$^{90}$ sequence also mediates an interaction between BLM and PCNA. We did identify an interaction of PCNA with the blm-QVF mutant and with an N-terminal truncation of BLM that is missing the first 160 amino acids, but not with a peptide of residues 1–120 of BLM (Supplemental Figure S3F). Thus, PCNA is indeed in a complex with BLM, but the PIP-box-like Mcm6-binding site is not involved in PCNA binding.

### A second site in BLM binds to the C-terminal winged-helix domain of Mcm6

In addition to the interaction of the N-terminal tail of BLM with the N-terminal domain of Mcm6, we identified a second interaction between the N-terminal tail of BLM and the C-terminal domain of Mcm6 (residues 325–821) (Figure 2B). Further dividing the Mcm6-C-terminal domain revealed a two-hybrid interaction between BLM residues 1–647 and Mcm6 residues 708–821 (Figure 2B, see also Supplemental Figure S3B–D), which make up the winged-helix (WH) domain that is required for MCM loading at origins [44–46]. BLM did not bind to the ATP-ase domain of Mcm6 (Figure 2B, residues 325–707; Supplemental Figure S3C) where most replisome components bind Mcm6, including Cdc45, TIM, TIPIN, Claspin, RPA2, MCM-BP and Mcm10 [47]. Further fragmenting the disordered tail of BLM, we determined that residues 220–285 of BLM bind to residues 708–821 of Mcm6 (Figure 2B, Supplemental Figure S3C). The most striking feature in this region of BLM is a stretch of four hydrophobic residues embedded in an acidic patch, $^{235}$VICI$^{238}$ in human BLM, that is conserved in mammals, birds and Xenopus (Figure 2D). Two additional hydrophobic residues nearby, W230 and L231 in human BLM, are conserved in mammals. Mutating the VICI or WLVICI residues to alanine (blm-VICI, blm-WLVICI) significantly reduced the two-hybrid interaction with Mcm6 (Figure 2F).

Based on where BLM binds Mcm6, we termed the BLM region that is important for association with the N-terminal domain of Mcm6 (disrupted by the blm-QVFF mutation) the Mcm6-N-terminal binding domain (MBD-N) and the BLM region that is important for association with the C-terminal domain of Mcm6 (disrupted by the blm-WLVICI mutation) the Mcm6-C-terminal binding domain (MBD-C).

### MBD-N and MBD-C of BLM act as G1- and S-phase-specific Mcm6-binding sites

Using reciprocal co-immunoprecipitations from synchronized $BLM^{+/+}$ cells (GM00637), we determined that wild-type BLM and Mcm6 interact at the G1/S boundary and in unperturbed S phase as well as in S-phase after induction of replication-dependent DSBs by camptothecin (CPT) (Figure 3A).

To assess the effect of the blm-QVFF and blm-WLVICI mutations on Mcm6 binding we used nuclear extracts of transiently transfected $BLM^{KO}$ cells (KSVS1452). The BLM mutants were expressed at similar levels to wildtype BLM (Supplemental Figure S4A). The blm-QVFF mutant failed to bind Mcm6 at the G1/S boundary, but co-immunoprecipitated normally with Mcm6 in S phase, including after CPT treatment (Figure 3B). In support of this G1-specific defect of the QVFF mutation, we observed the same Mcm6-binding pattern for an N-terminal truncation of BLM that removes the QVFF residues (blm-Δ160) (Supplemental Figure S4C) and for the milder blm-QVF mutation, which retains some Mcm6 binding in G1 (Supplemental Figure S4B). Intriguingly, the blm-WLVICI mutation had the opposite effect; blm-WLVICI bound Mcm6 normally at the G1/S boundary, but poorly in S phase and after exposure to CPT (Figure 3C). The milder VICI mutation retained slightly more interaction with Mcm6 in S-phase and after CPT treatment (Supplemental Figure S4D). Thus, BLM uses two distinct sites—residues 83–90 (MBD-N) and residues 231–238 (MBD-C)—to bind to
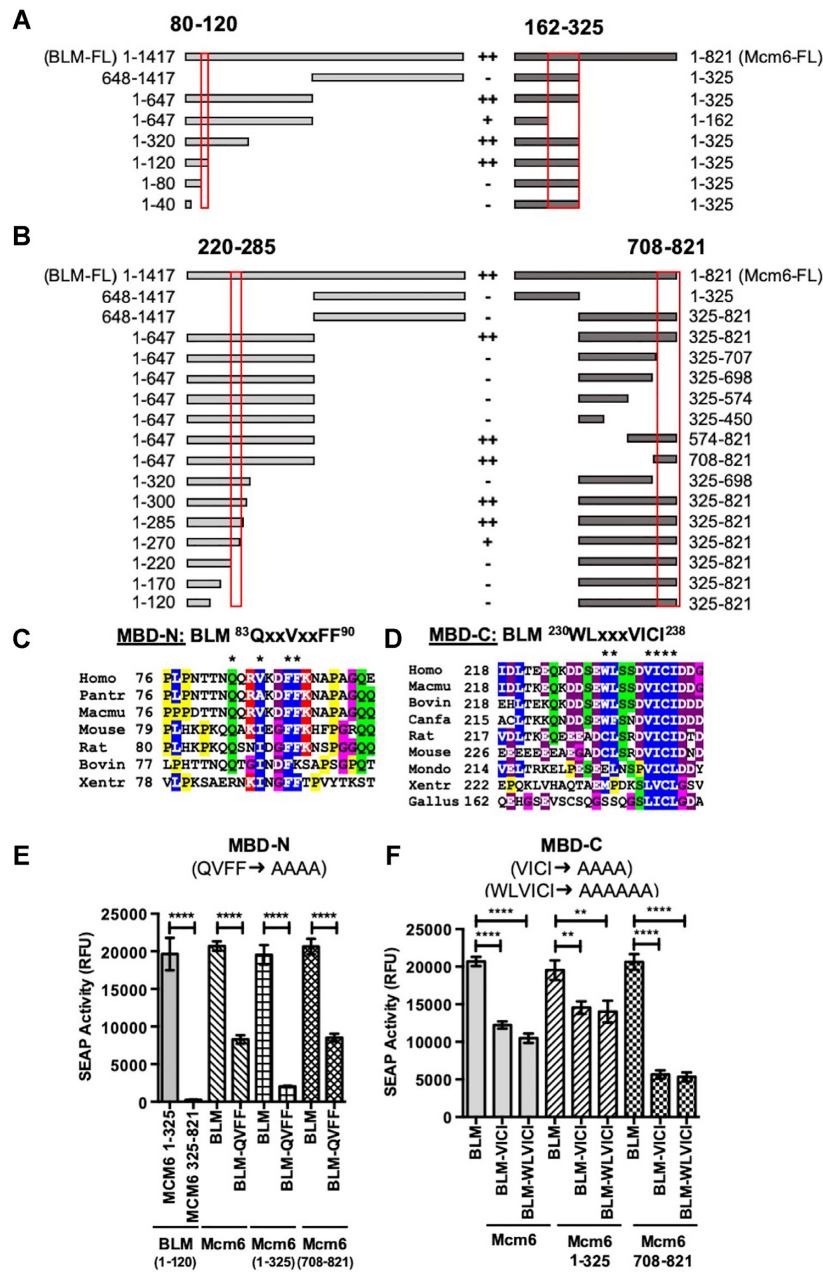
**Figure 2.** Two distinct sites in the BLM disordered N-terminal tail interact with Mcm6. (**A**) Mammalian two-hybrid assay was performed with N-terminal fragments of BLM and Mcm6 (See also Supplemental Figure S3B). Red boxes indicate interacting sites on BLM and Mcm6. Interactions are labeled with ++ (strong) and + (weak), and lack of interaction is labeled with a minus sign. (**B**) Mammalian two-hybrid assay was performed with N-terminal fragments of BLM and Mcm6 (see also Supplemental Figure S3C). Red boxes indicate interacting sites on BLM and Mcm6. Interactions are labeled with ++ (strong) and + (weak), and lack of interaction is labeled with a minus sign. (**C**) Alignment of residues 76–98 of human BLM containing MBD-N with corresponding regions of BLM from other mammals and *Xenopus trop.* Residues in this disordered region showing conservation across at least some species are colored. Proline and glycine residues typical for disordered regions are also highlighted. Residues labeled with a star were mutated to alanine (QVFF → AAAA) (see Figure 2E). MBD-N, Mcm6-N-terminal binding site. (**D**) Alignment of residues 218–241 of human BLM containing MBD-C with corresponding regions of BLM from other mammals, *Xenopus trop.* and chicken. Hydrophobic and acidic residues are colored blue and purple, respectively. Other residues showing conservation across at least some species are colored green. Proline and glycine residues typical for disordered regions are yellow. Residues labeled with a star were mutated to alanine (WLVICI → AAAAAA) (see Figure 2F). MBD-C, Mcm6-C-terminal binding site. (**E**) Mammalian two-hybrid assay was performed in KSVS1452 (*BLM^{KO}*) cells expressing full-length BLM carrying the QVFF/AAAA mutation (blm-QVFF) and full-length Mcm6 or Mcm6 fragments. (**F**) Mammalian two-hybrid assay was performed in KSVS1452 (*BLM^{KO}*) cells expressing full-length BLM carrying the VICI/AAAA (blm-VICI) or WLVICI/AAAAAA (blm-WLVICI) mutations and full-length Mcm6 or Mcm6 fragments. Differences between means were analyzed by a *t*-test and presented as ** ($P < 0.01$) and ****($P < 0.0001$).
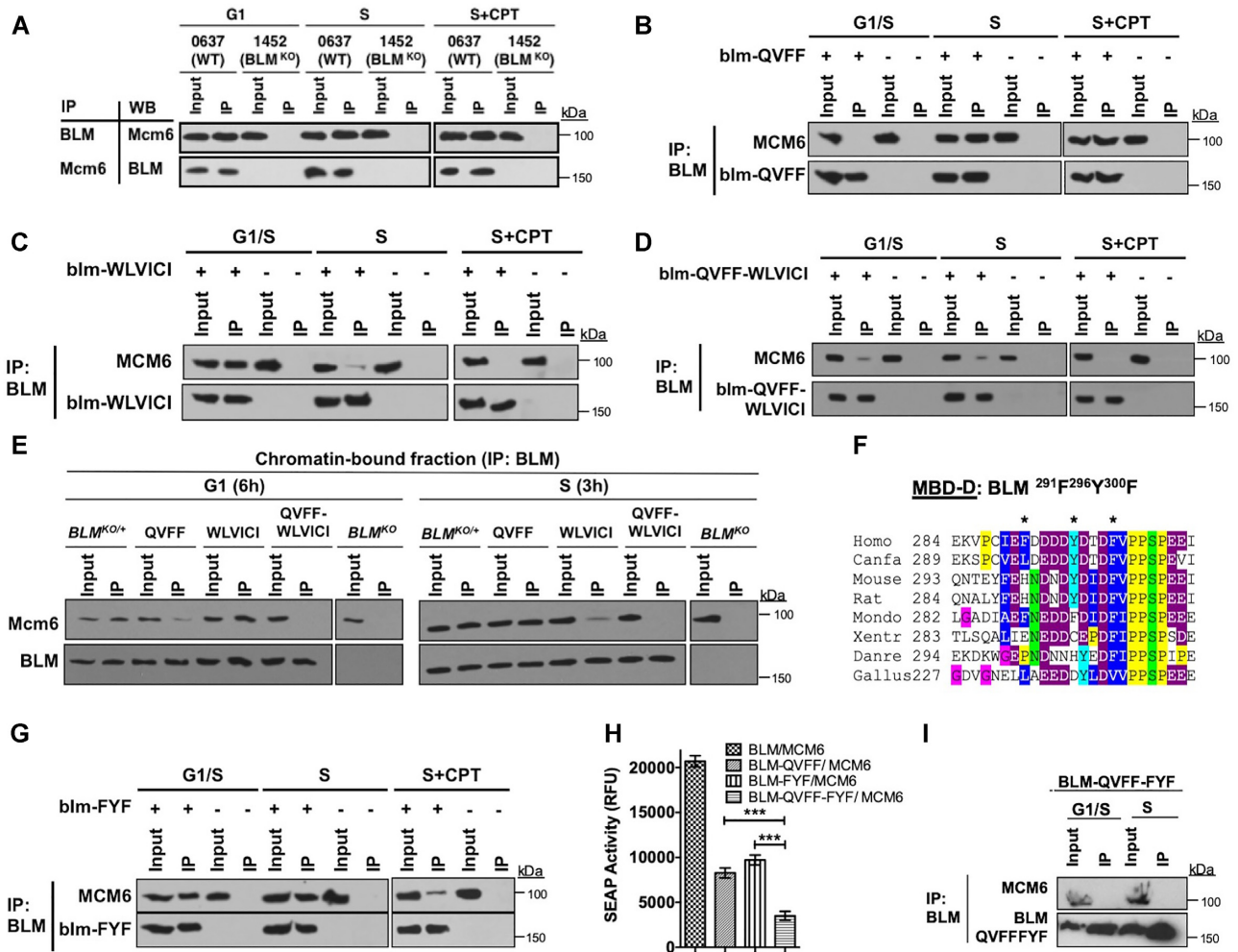
**Figure 3.** BLM binds Mcm6 though different sites in unperturbed G1, S-phase, and after DNA damage. (**A**) GM00637 (WT) and KSVS1452 (*BLM^KO*) cells were synchronized at the G1/S boundary, released into S-phase for 3 hours, exposed to 1μM camptothecin (CPT) for 1 h and released into fresh media for 45 min. Reciprocal co-immunoprecipitations of endogenous BLM and Mcm6 were performed at G1/S, in S-phase and during recovery from CPT. (**B–D**) KSVS1452 (*BLM^KO*) cells transiently expressing BLM mutants were synchronized at G1/S, released into S-phase for 3 h, exposed to CPT for 1 h, released for 45 min, and the interaction between BLM mutants and endogenous Mcm6 assessed by co-immunoprecipitation. (**E**) Co-immunoprecipitation of chromatin-bound BLM and Mcm6. Chromatin-bound protein fraction was extracted from cells stably expressing BLM mutants (see Supplemental Table S1) 6 h after release from nocodazole block (G1 phase) or 3 h after release from G1/S boundary (S-phase). (**F**) Sequence alignment of residues 284–308 of human BLM and BLM homologs from other vertebrates. Residues mutated in the blm-FYF mutant (MBD-D) are labeled with a star. MBD-D, DNA-damage-induced Mcm6-binding site. (**G**) Co-immunoprecipitations between full-length BLM carrying the FYF mutation and Mcm6 were performed as in (B–D). (**H**) Mammalian two-hybrid assay to assess the effect of the blm-FYF and blm-QVFF-FYF mutations on the BLM/Mcm6 interaction. Mean ± SD is shown. Differences between means were analyzed by a *t*-test and presented as *** ($P < 0.001$). (**I**) Co-immunoprecipitations between full-length BLM carrying the QVFF and FYF mutations and Mcm6 were performed as in (B–D).

Mcm6 in G1 and in S-phase, respectively. Indeed, generating the MBD-N/MBD-C double mutant (blm-QVFF-WLVICI) disrupted the BLM/Mcm6 interaction in both G1 and S-phase as well as under DNA-damaging conditions (Figure 3D). In the chromatin fraction, we observed the same requirement of MBD-N and MBD-C for cell cycle phase specific association of BLM with Mcm6 (Figure 3E).

Since the BLM N-terminal tail is disordered and, thus, sequence conservation is low, an acidic patch with several hydrophobic residues (^291FDDDDYDTDF^300) just downstream of MBD-C stood out (Figure 3F). Nearby S304 had previously been shown to be phosphorylated in S-phase where it is involved in binding TopBP1 (48,49). Using transient transfections of *BLM^KO* cells (KSVS1452),

we found that mutating BLM residues F291/Y296/F300 to alanine (blm-FYF) had no effect on binding endogenous TopBP1 in unperturbed S-phase, but reduced TopBP1 binding after CPT exposure (Supplemental Figure S4E). Similar to TopBP1, Mcm6 immunoprecipitated with blm-FYF in unperturbed S phase, but lost most of its association after exposure to CPT (Figure 3G). In contrast to the BLM/Mcm6 interaction, however, the first 240 residues of BLM, which contain the Mcm6 binding sites, were not sufficient for the BLM/TopBP1 interaction (Supplemental Figure S4F), thus separating TopBP1- and Mcm6-binding requirements for BLM. The FYF mutation significantly reduced the two-hybrid interaction between BLM and Mcm6, and mutating both QVFF and FYF led to a further reduc-

tion (Figure 3H). Interestingly, the blm-QVFF-FYF double mutant completely failed to immunoprecipitate Mcm6 at G1/S and in S phase (Figure 3I), suggesting that in unperturbed S phase residues 83–90 (MBD-N) and 291–300 (FYF) of BLM contribute to Mcm6 binding, but that binding through one of these sites is sufficient for BLM association with Mcm6 as long as the major BLM/Mcm6 binding site in S-phase, residues 230–238 (MBD-C), is intact. Since the FYF mutation interrupted BLM/Mcm6 binding in response to DNA damage we termed the interaction site the DNA-damage-dependent Mcm6-binding site, MBD-D.

We verified the importance of MBD-N, MBD-C and MBD-D for G1- and S-phase specific association of BLM with Mcm6 using fluorescence microscopy of *BLM^{KO}* cells (KSVS1452) transfected with plasmids expressing the BLM mutants (Supplemental Figure S5). Consistent with co-immunoprecipitations, the blm-QVFF mutation impaired BLM/Mcm6 colocalization in G1, whereas the blm-WLVICI mutation had a wildtype phenotype in G1, but disrupted colocalization in S-phase. As expected, the blm-QVFF-FYF mutation had the most dramatic effect, disrupting colocalization with Mcm6 in G1 and in S-phase and after CPT exposure (Supplemental Figure S5).

Finally, we observed that besides Mcm6, BLM also showed weaker interactions with Mcm2 and Mcm7 in G1 and in S-phase whereas Mcm3,4,5 could not be detected, both in the soluble and chromatin-bound fractions (Supplemental Figure S4G and FigureS4I). This pattern is similar to co-immunoprecipitation of Mcm6, which yielded Mcm2,7 and to a lesser extent Mcm3,4,5 (Supplemental Figure S4H). This suggests that Mcm2 and Mcm7 may have co-immunoprecipitated with BLM via their association with Mcm6 whereas the less tight association of Mcm3,4,5 with Mcm6 may have prevented their detection in the BLM co-immunoprecipitate. Alternatively, BLM might directly contact Mcm2 and Mcm7 besides Mcm6 in a manner similar to that of other MCM interacting proteins, such as Cdt1 and Mcm10, which bind strongly to Mcm6 and Mcm2, respectively, and also interact with other MCM subunits, but not all (50,51).

### Mutation of BLM/Mcm6 interaction sites causes a 'Slow DNA break repair' phenotype

To assess the importance of the BLM/Mcm6 interaction for the repair of replication-associated DSBs, we generated KSVS1452 (*BLM^{KO}*) cells stably expressing BLM mutant cDNAs (Supplemental Figure S4J), synchronized them at the G1/S boundary, released them into S-phase for three hours and exposed them to a low dose of CPT for one hour. We then measured the efficiency of DSB repair 24 and 48 h after release from CPT using the neutral comet assay. Cells expressing the G1-specific blm-QVFF mutation repaired DSBs efficiently whereas cells expressing the S-phase-specific blm-WLVICI mutation had a higher amount of unrepaired DSBs than wildtype BLM cells 48 h after CPT removal (Figure 4A), suggesting that the association of BLM with Mcm6 in S-phase contributes to BLM's role in the repair of replication-dependent DSBs. The blm-QVFF-FYF mutation, which completely disrupts

co-immunoprecipitation and colocalization of BLM with Mcm6 in S-phase, repaired DSBs as inefficiently as cells not expressing BLM. The severity of this DSB repair defect is most likely due to the particular importance of MBD-D during the DNA damage response, not only for the interaction of BLM with Mcm6, but also with TopBP1 (Supplemental Figure S4E).

### Response to DNA-damage and replication stress differentially depends on MBD-N/C/D

Cells lacking BLM or BLM helicase activity are hypersensitive to genotoxins, including hydroxyurea (52,53), which impairs DNA synthesis by depleting the nucleotide pool. Here, we observed that those BLM mutations that interrupt the interaction with Mcm6 in S-phase (blm-WLVICI, blm-FYF, blm-QLFF-FYF, blm-QVFF-WLVICI) caused significantly increased sensitivity to hydroxyurea, whereas the blm-QVFF mutation, which primarily affects Mcm6 binding in G1, exhibited a phenotype similar to cells complemented with wildtype BLM (Figure 4B).

BLM is also one of three mammalian DNA helicases (WRN, FANCJ) currently implicated in G-quadruplex unwinding *in vivo* (54–56). Staining of cells with a G-quadruplex (G4)-specific antibody increases in the absence of BLM and upon exposure to the G4-stabilizer pyridostatin (PDS) (19). PDS induces replication-dependent DNA damage in S-phase and transcription-dependent DNA damage in G1 (57). Here, we found that all BLM mutations that disrupt Mcm6 binding caused significant decrease in survival after exposure to PDS, including the G1-specific blm-QVFF mutation (Figure 4C). Combining the blm-QVFF mutation with either the WLVICI or FYF mutations, which fully disrupts BLM/MCM association in G1 and in S-phase as well as after DNA-damage exposure, caused PDS hypersensitivity greater than either single mutant and was comparable to cells not expressing BLM (Figure 4C). Taken together, these findings show that the Mcm6-binding sites of BLM play essential roles in the cellular response to HU and PDS and suggest that MBD-N plays a role in the repair of G4-ligand induced DNA-damage in G1-phase, but not in the response to replication stress in S-phase.

### Uncoupling of BLM and Mcm6 in S-phase causes BLM-helicase-dependent acceleration of DNA replication speed

Cells from Bloom syndrome patients exhibit reduced replication fork speed (58,59). To gain insight into the importance of the interaction between the BLM and MCM helicases for DNA replication we utilized single-molecule DNA fiber analysis. To do so, we labeled sites of ongoing DNA replication by incubating unperturbed cells with CIdU for 30 min and then, after washing, with IdU for an additional 30 minutes. Measuring the length of IdU-labeled DNA adjacent to CIdU-labeled DNA (elongating replication forks) on stretched DNA fibers, we observed a significant increase in replication speed in cells that stably expressed the blm-WLVICI mutation, which interrupts BLM-Mcm6 interaction in S-phase (Figure 5A). The blm-QVFF-WLVICI double mutant also exhibited significantly faster
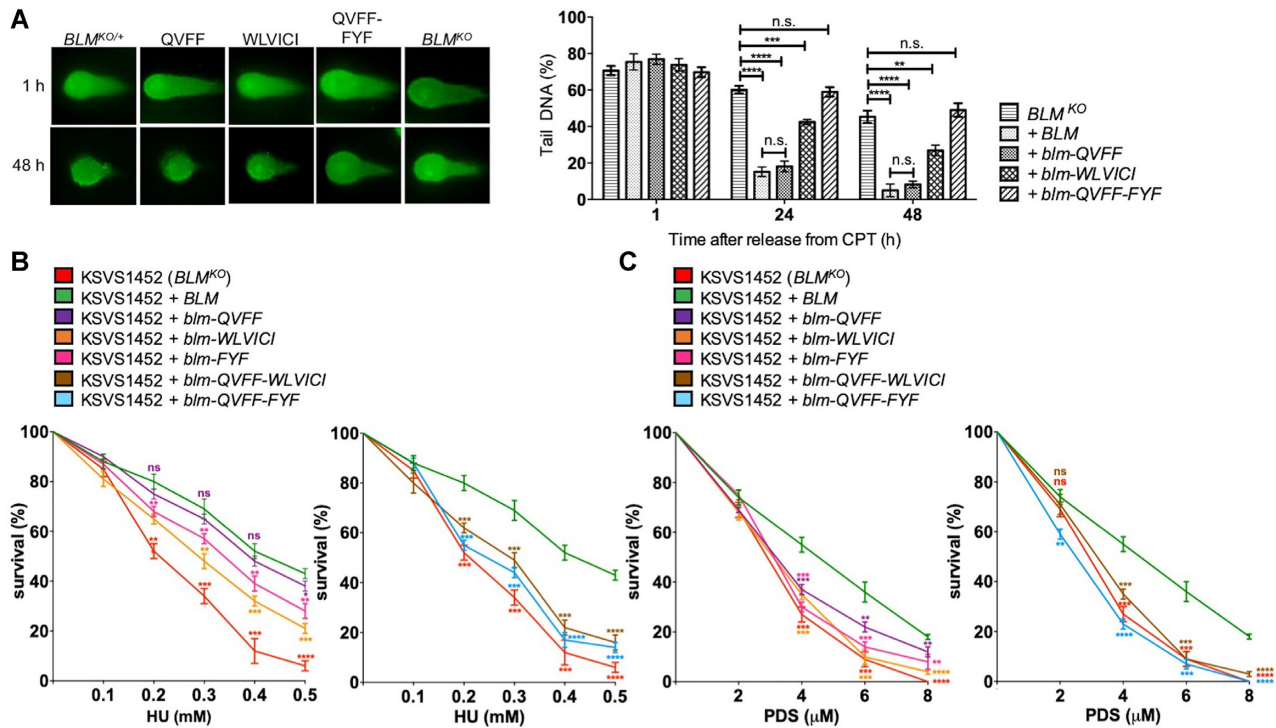
**Figure 4.** BLM/Mcm6 interaction contributes to the DNA damage response. (**A**) *BLM^KO* cells (KSVS1452) stably expressing BLM (+*BLM*) or BLM mutants were synchronized at G1/S, released into S-phase for 3 h and exposed to 1 μM camptothecin (CPT) for 1 h to induce replication-dependent DSBs. Repair of DSBs was assessed 24 and 48 h after release from CPT using a neutral comet assay as previously described (53). At least 50 comets were imaged for three stable clones of each BLM mutant for a minimum of 150 comets per cell line at each time point. Mean ± SD is reported. ** $P < 0.01$, *** $P < 0.001$, **** $P < 0.0001$. (B, C) Clonogenic assays were performed to measure survival of stable cell lines derived from KSVS1452 stably expressing full length BLM with mutations that disrupt Mcm6 binding. Cells were exposed to increasing concentrations of (**B**) hydroxyurea (HU) and (**C**) pyridostatin (PDS). Assays were performed on three stable clones for each BLM mutant and cell survival (%) is reported as mean ± SD. A *t*-test was performed to determine statistical significance of differences between the BLM-complemented cell line (+BLM) and the mutant cell lines: ** $P < 0.01$, *** $P < 0.001$, **** $P < 0.0001$; ns, not significant.

DNA replication speed. Like the WLVICI mutation, the QVFF-FYF mutation disrupts BLM/Mcm6 interaction in S-phase and caused a significant increase in DNA replication speed (Supplemental Figure S6A). In contrast, the blm-QVFF mutation, which interrupts the BLM/Mcm6 interaction only in G1, did not lead to increased DNA replication speed (Figure 5A). We confirmed that the WLVICI mutation did not affect the ability of BLM to bind other proteins known to interact with BLM (Supplemental Figure S6C). Calculating the ratio between the length of CIdU and IdU-labeled DNA, we show that any changes in DNA replication speed were equal during the two labeling periods (Supplemental Figure S7).

Increased DNA replication speed may be caused by increased fork rate or by increased origin firing. Since BLM-deficiency has previously been shown to lead to increased origin firing (11), we assessed origin firing by measuring the fraction of DNA fibers that had incorporated only IdU, indicating new origins that had fired during the second labeling pulse. The analysis showed increased origin firing in *BLM^KO* cells, consistent with previous reports in BLM-deficient cells (11), but not in the blm-WLVICI mutant (Figure 5C), suggesting that the BLM/Mcm6 interaction regulates replication speed by regulating fork movement. That Bloom-syndrome-patient-derived cell lines, which are

BLM-deficient, and the *BLM^KO* cell line (KSVS1452) constructed in our laboratory (30) did not exhibit accelerated DNA replication (58,59) (Figure 5A) further suggests that increased replication speed in the blm-WLVICI and blm-QVFF-FYF mutants requires the BLM protein. This raised the possibility that the helicase activity of BLM was responsible for the increased replication speed in cells where BLM had become uncoupled from MCM in S-phase. If true, a K695R mutation, which disrupts the helicase activity of BLM (2), should reduce the replication speed in the blm-WLVICI mutant cell line. Indeed, the increase in replication speed caused by the WLVICI mutation was eliminated by introducing the K695R mutation (Figure 5B). In fact, replication speed in cells stably expressing the blm-WLVICI-K695R mutation (Supplemental Figure S4K) was the same as that of cells expressing the blm-K695R mutation or expressing no BLM (Figure 5C). We obtained the same result when measuring replication speed in another stable clone of KSVS1452 expressing the blm-WLVICI-K95R mutant (Supplemental Figure S6B) and in KSVS1452 (*BLM^KO*) cells transiently transfected with plasmids expressing the WLVICI and WLVICI-K695R mutants of BLM (Supplemental Figure S6F and G). In contrast to cells that exhibit increased replication speed due to PARP1 inhibition (60), increased replication speed in the blm-WLVICI and blm-
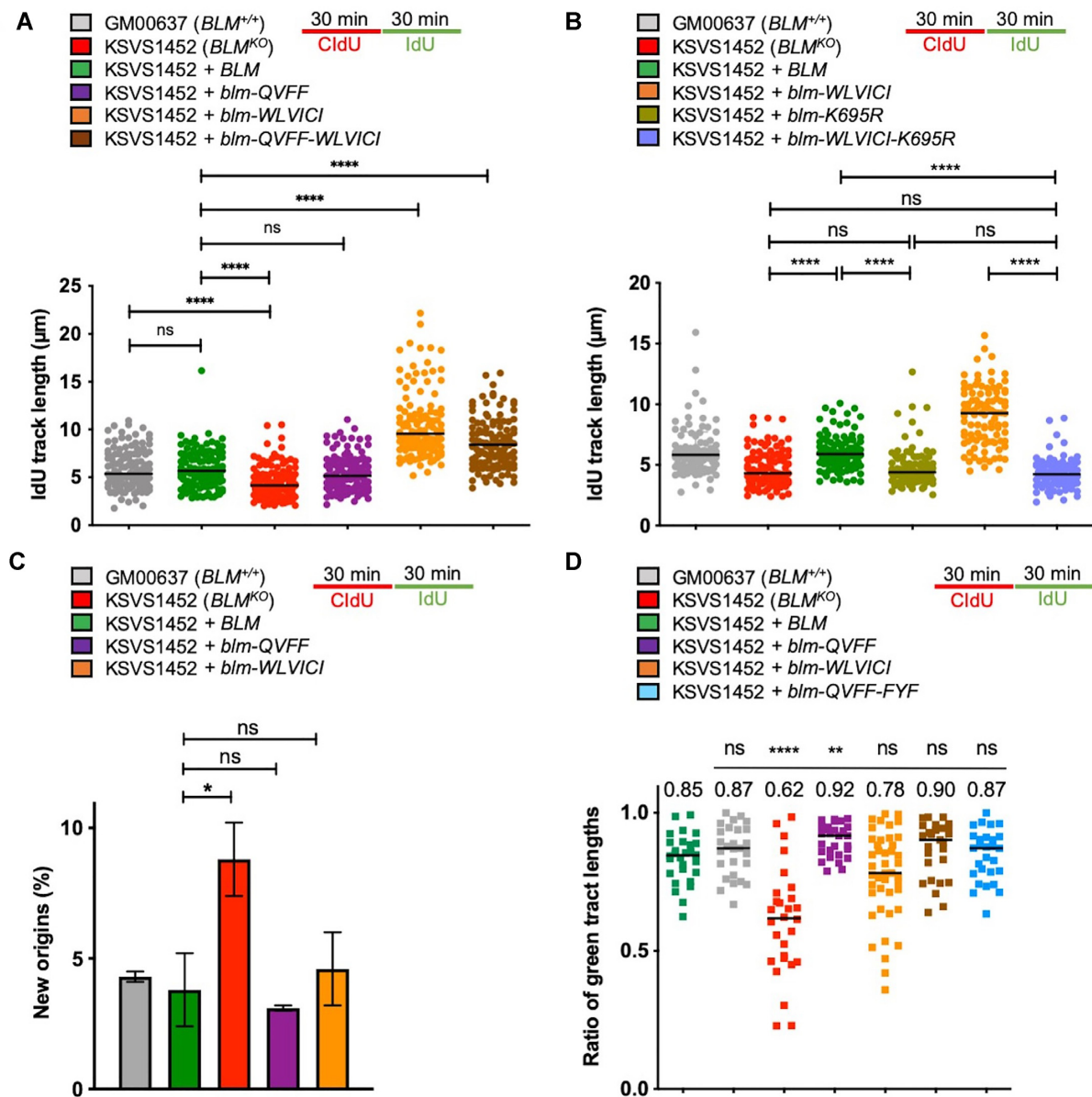
**Figure 5.** Uncoupling of BLM from Mcm6 in S-phase causes BLM-helicase-dependent acceleration of DNA replication speed. (**A**) DNA fiber analysis was used to compare replication speed between $BLM^{KO}$ cells (KSVS1452) complemented with wildtype BLM or BLM mutants that fail to bind Mcm6 in S phase (blm-WLVICI), in G1 phase (blm-QVFF), or in G1 and S-phase (blm-QVFF-FYF). Unperturbed cells were incubated in the presence of CIdU for 30 min and then in the presence of IdU for 30 min, immunostained and imaged on a Keyence fluorescence microscope. A minimum of 100 fibers showing a red region extended by a green region (elongating forks) were analyzed for each cell line, and the length ($\mu$m) of the green (IdU) region served as a measure of replication speed. A Mann-Whitney test was performed to determine statistical significance of IdU track length differences between the wildtype BLM-complemented cell line (+BLM) and the mutant BLM cell lines: **** $P < 0.0001$; ns, not significant. (**B**) DNA fiber analysis was used to compare replication speed between $BLM^{KO}$ cells (KSVS1452) stably expressing *blm-WLVICI*, *blm-K695R* (clone #13), or *blm-WLVICI-K695R* (clone #11) alleles of BLM. A minimum of 100 fibers were imaged and analyzed as in (A). (**C**) New origin firing was measured in BLM wildtype cells (GM00637), $BLM^{KO}$ cells (KSVS1452), and $BLM^{KO}$ cells (KSVS1452) complemented with wildtype BLM or BLM mutants that fail to bind Mcm6 in S phase (blm-WLVICI) or in G1 phase (blm-QVFF). A minimum of 200 DNA fibers from three different experiments were imaged as in *(B)* and the fraction of DNA fibers only stained with IdU (indicative of origin activation during the second labeling pulse) determined. A *t*-test was performed to determine statistical significance of differences between the BLM-complemented cell line (+BLM) and the mutant cell lines: * $P < 0.05$; ns, not significant. (**D**) Sister fork asymmetry was determined in BLM-proficient and blm-mutant cell lines by determining the ratio between the length of IdU labels on sister forks; i.e, two IdU labels extending from the same CIdU label. Between 25–40 sister forks per cell line were analyzed. Median ratio is indicated above the scatter dot blot. A Mann-Whitney test was performed to determine statistical significance of differences between the BLM-complemented cell line (+BLM) and the mutant cell lines. ** $P < 0.01$, **** $P < 0.0001$; ns, not significant.

QVFF-FYF mutants did not activate the DNA-damage checkpoint (Supplemental Figure S6E).

Finally, we assessed sister fork asymmetry, a measure of fork stalling (61), by calculating the ratio between the length of the IdU labels on bidirectional forks. Whereas sister forks in *BLM^KO* cells showed a significant decrease in the ratio of IdU label lengths, indicative of greater fork stalling than in the parental BLM-proficient cell line (GM00637), the blm mutants did not exhibit significant decreases in IdU label ratios (Figure 5D), suggesting that BLM mutations that interrupt the interaction with Mcm6 do not lead to increased replication fork stalling.

## DISCUSSION

In this study, we have identified a direct physical interaction between the BLM helicase and the MCM helicase subunit Mcm6 and show that coupling BLM to Mcm6 in S-phase is necessary for maintaining normal replication speed. Acceleration of replication speed upon uncoupling of the two DNA helicases depends on the helicase activity of BLM.

The N-terminal tail of BLM contains the Mcm6-binding region with two distinct binding sites, MBD-N and MBD-C, that differentially mediate Mcm6 binding in unperturbed G1 and S-phase, respectively. A third site (MBD-D) contributes to Mcm6 binding after DNA damage, but is dispensable for BLM/Mcm6 interaction during the unperturbed cell cycle. Whereas the BLM/Mcm6 interaction needs to be maintained only in S-phase for survival after HU-induced replication stress, it is required for cell survival after exposure to the G4-ligand pyridostatin in both G1 and S-phase, demonstrating the importance of the BLM/Mcm6 interaction for the response to genotoxins during DNA replication and pointing to a possible new role for BLM in DNA-damage repair in G1 phase. The blm-QVFF-FYF and blm-QVFF-WLVICI mutations, which disrupt the BLM/Mcm6 interaction throughout the cell cycle, render cells as sensitive to DNA damage induced by pyridostatin as cells not expressing BLM (Figure 4C), highlighting the role of the BLM/MCM interaction in the response to DNA damage.

Currently, BLM function is defined by its roles in DSB repair by homologous recombination, and during the replication stress response when it assembles with Topo IIIα and Rmi1/2 at sites of stalled replication forks and functions with FANCD2 in replication fork restart and dormant origin suppression (10,11,59,62). Previous studies have mostly focused on exposing BLM-deficient cells to DNA damage or replication stress. Using point mutants of BLM, we now find that BLM also plays an important role during DNA replication in the absence of exogenous DNA damage or induced replication stress. We show that disrupting the BLM/Mcm6 interaction during S-phase in unperturbed cells triggers supra-normal replication speed. Such abnormally high replication speed was recently shown to reduce the ability of cells to detect and repair DNA damage and decrease the survival of HR-deficient cancer cells (60). However, we did not detect activation of the DNA damage checkpoint in cells with increased replication speed due to mutations in BLM. This suggests that during accelerated replication upon uncoupling of BLM from Mcm6, single-stranded DNA at the replication fork or DNA damage are

not formed at levels that cause checkpoint activation. It remains to be determined, however, if the increased replication speed in BLM mutant cells gives rise to genome instability.

Disruption of the BLM/Mcm6 interaction by the blm-WLVICI and blm-QVFF-FYF mutations cannot be solely responsible for the increased replication speed since a deletion of the *BLM* gene would be expected to have the same effect as disrupting the BLM/Mcm6 interaction. However, neither cells from Bloom syndrome patients (58,59) nor a cell line where we disrupted the *BLM* gene showed increased replication speed (Figure 5B), establishing that the higher speed of replication upon disruption of the BLM/Mcm6 interaction requires the BLM protein. Indeed, we determined that the helicase activity of BLM is essential for the increased replication speed after uncoupling BLM from Mcm6.

BLM possesses excellent G-quadruplex (G4) unwinding activity (54,55) and can resolve R-loops (24), which could allow the replication fork to move faster by aiding it through genomic sites that adopt unusual secondary structures. BLM could also promote fork progression by preventing secondary structure formation in the unwound DNA behind the CMG helicase. Like several other DNA helicases, BLM is also able to reverse replication forks *in vitro* and can restore functional replication forks by resolving four-way junctions that may form at stalled forks (14,63). Indeed, fewer forks restart after DNA damage in BLM-deficient cells (11) and it is possible that this requirement of BLM for fork restoration extends to replication in unperturbed cells. Our findings suggest that such BLM activities that can accelerate replication speed need to be coupled to Mcm6 binding in order to maintain the normal speed of DNA replication. Additionally, BLM could increase replication speed indirectly, for example through any of its known interactions with DNA repair factors and checkpoint components or by affecting origin usage, which is linked to fork speed (64,65). However, our analysis of new origin firing, although limited, indicates that the BLM mutations that disrupt Mcm6 binding do not alter origin activity.

Thus, a model emerges wherein BLM helicase activity accelerates replication fork progression, most likely by assisting the replicative CMG helicase with unwinding unusual secondary structures, and tethering BLM to MCM via its long N-terminal tail limits this activity to the immediate vicinity of the replisome, ensuring normal replication speed (Figure 6D). When BLM becomes untethered from MCM, its unwinding activity is unrestrained, which allows the replisome to accelerate.

This novel role of BLM in unperturbed S-phase is unlikely to extend to G1 when DNA replication is absent. Our findings suggest that BLM is not simply being loaded into the pre-initiation complex in G1 as the blm-QVFF mutant, which fails to interact with Mcm6 in G1-phase, can still associate with Mcm6 in S-phase. We can envisage two functions for BLM and the BLM/Mcm6 association in G1. First, after continual loading at ORC-binding sites, MCMs translocate to be distributed throughout the genome far in excess of and away from ORC-binding sites prior to initiation of DNA replication (66). BLM binding to Mcm6 could contribute to this movement of MCMs on
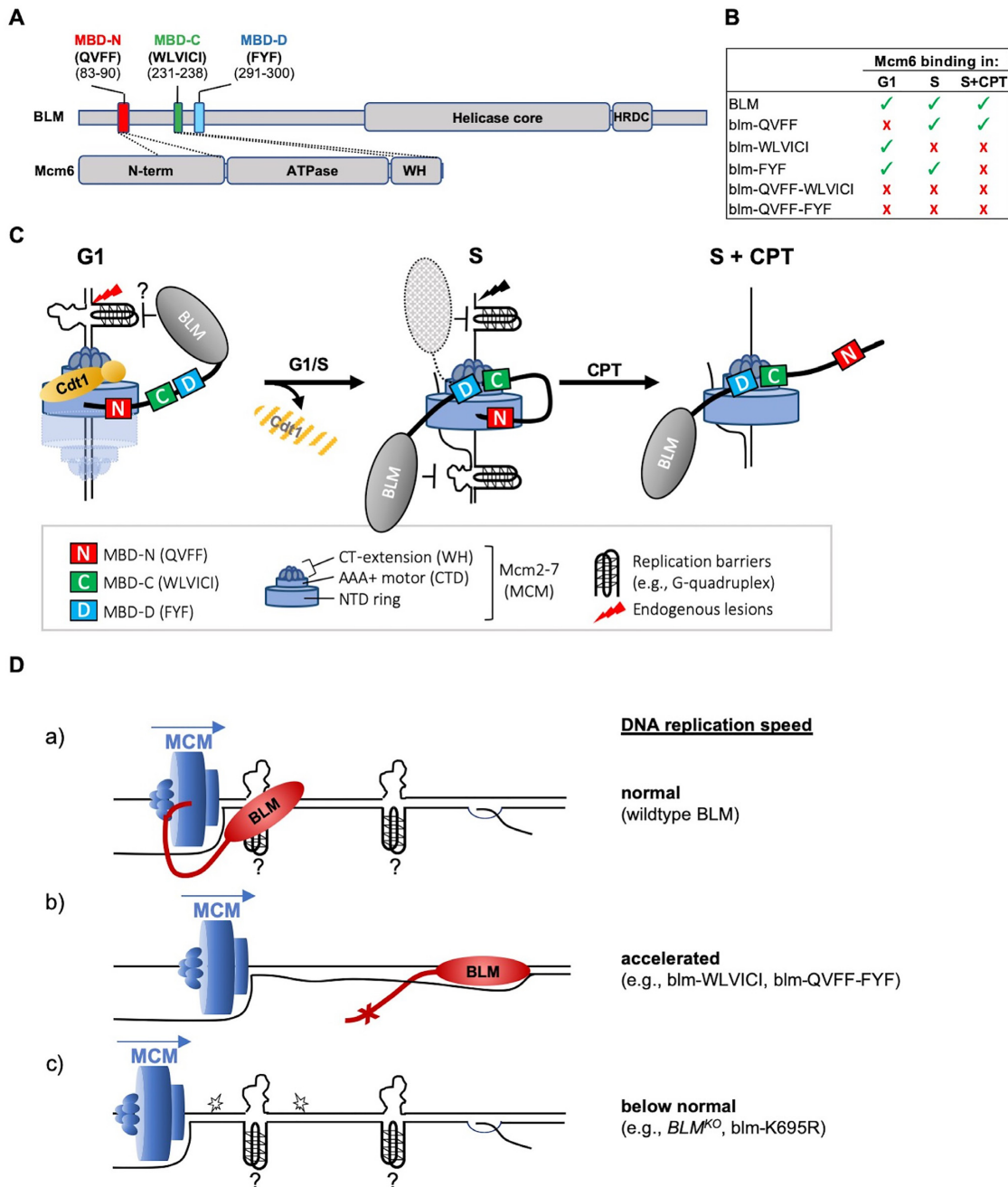
**Figure 6.** Cell-cycle regulated BLM/Mcm6 interaction and function (**A**) Identification of three binding sites in the disordered N-terminus of BLM that facilitate binding to Mcm6 in G1 phase (MBD-N, residues 83–90), in unperturbed S-phase (MBD-C, residues 230–238) and after DNA damage (MBD-D, residues 291–300). (**B**) Effect of BLM mutations identified in this study on the BLM/Mcm6 interaction in G1, in S-phase, and in S-phase after CPT exposure. (**C**) Proposed model for cell-cycle-dependent BLM/Mcm6 interaction: In G1, BLM binds the N-terminal domain of Mcm6 via MBD-N, leaving the Mcm6 C-terminus free to bind Cdt1 for pre-RC formation. MBD-C and MBD-D of BLM are not required for Mcm6 binding in G1. The role of the BLM/Mcm6 interaction in G1 phase is unclear; BLM might function in G1 to facilitate the long-range re-distribution of MCMs away from ORC-binding sites by removing DNA secondary structures or other obstacles. On S-phase entry, Cdt1 is rapidly degraded and BLM engages Mcm6 through MBD-C. Binding via MBD-C is necessary for Mcm6 interaction in S-phase but not sufficient; at least one other site, MBD-N or MBD-D, has to contribute to stabilize binding. BLM may associate with MCM in S-phase to target the unfolding of CMG-blocking DNA structures, such as G4s and R-loops, to the duplex DNA immediately ahead of the fork and prevent it from colliding with obstacles and stalling. BLM binding to Mcm6 during unperturbed S-phase would also increase BLM availability at the fork to deal with replication stress or DNA damage. During exposure of cells to CPT, BLM/Mcm6 interaction is mediated by MBD-C binding to the C-terminal extension of Mcm6 and by MBD-D. MBD-N plays only a minor role in the DNA-damage response, making the region of BLM containing MBD-N (residues 1–230 residues) available to interact with DNA repair factors or checkpoint components. (**D**) Role of the BLM/Mcm6 interaction as a negative regulator of replication speed: (a) In wildtype cells, BLM helicase activity for unwinding blocking DNA structures (e.g. G-quadruplexes, R-loops) is restricted to the immediate vicinity of the replisome by tethering BLM to Mcm6. (b) If BLM is untethered from Mcm6, BLM helicase activity is no longer restricted, allowing the replisome to move faster. The 'x' indicates mutation of an Mcm6 binding site. (**C**) In the absence of BLM or BLM helicase activity, slower replisome progression may be caused by DNA structures, such as G4 structures or R-loops, that cannot be unwound in a timely manner and by reactive oxygen species (indicated by stars) (30).

DNA by removing DNA secondary structures and other obstacles. Although RecQL4, another RecQ-like helicase, is essential for the initiation of DNA replication in human cells (67), it lacks the conserved RQC domain that enables BLM and WRN to unwind DNA secondary structures such as G4s, and RecQ4 is unable to unwind these structures *in vitro* (68). In a second, not mutually exclusive, scenario, BLM could function in G1 phase to unwind DNA secondary structures to prevent transcription-dependent DNA damage (21). G4 structures and PDS exposure not only impair replisome progression in S-phase and induce replication-dependent DNA damage, they can also induce transcription-dependent DNA damage in G1 (69). Moreover, BLM's ability to resolve transcription intermediates, such as R-loops (24), might be needed in G1 phase. That loaded MCMs are distributed by active transcription to non-transcribed genes and intergenic regions of the genome prior to the G1/S transition (70) may provide a link between such a transcription-related function of BLM and Mcm6 in G1.

Further, we show that the physical interaction between BLM and Mcm6 is complex, involving three different sites on BLM in different combinations and at least two different sites in Mcm6, depending on cell cycle phase and DNA-damage exposure. We propose a model for the regulation of the BLM/Mcm6 interaction (Figure 6) wherein MBD-N of BLM associates with the N-terminus of Mcm6 in G1 phase, leaving the ATPase domain and C-terminal domain of Mcm6 free for other pre-RC and pre-IC components to bind. For example, Cdc45, RPA2, TIM, TIPIN, MCM10 and MCM-BP bind to the ATPase domain of Mcm6, and Cdt1 is bound to the C-terminus of Mcm6 for the recruitment of MCM hexamers to ORC (47). In S-phase, Mcm6 no longer binds Cdt1 (Supplemental Figure S6D) and Cdt1 is rapidly degraded (71–73), allowing BLM to bind to the Cdt1-binding domain of Mcm6 via MBD-C. Upon induction of DSBs, BLM engages Mcm6 at a third site, MBD-D. Interestingly, MBD-C is necessary for the BLM/Mcm6 interaction in S-phase but not sufficient, requiring the contribution from at least one of the other two binding sites, either MBD-N or MBD-D, to maintain Mcm6 binding. This optional involvement of MBD-N in unperturbed S-phase and after DSB induction frees up binding sites in the first 230 residues of BLM for several DNA repair and checkpoint proteins that may be required for BLM functions in normal S-phase and during the response to DNA damage, including Topo IIIα/Rmi1/Rmi2, RPA, Rad51 or p53 (15,74,75).

In addition to binding an increasing number of proteins with functions in DNA repair, recombination and replication, the N-terminal tail of BLM is SUMOylated at lysines 317,331, 344 and 347. Non-covalent binding of SUMO by BLM residues V235/I236 and nearby residues I218/L220 has been shown to be important for these sumoylation events (76). Interestingly, this SUMO-binding site, which resembles an inverted SUMO-binding motif 2 (SBM2, [V/I][V/I]X[V/I]) (77), resides within MBD-C and overlaps with the Mcm6 binding site. The possibility that MBD-C contains a SUMO-binding motif raises the possibility that the MBD-C-mediated BLM/Mcm6 interaction might be regulated by the sumoylation status of Mcm6. In yeast, there is evidence of Mcm6 being SUMOylated in G1 and this sumoylation playing a regulatory role by counteract-

ing MCM phosphorylation to impair replication initiation (78). However, it is currently unknown if human Mcm6 is SUMOylated, and if so, whether sumoylation plays a similar role in the G1/S transition.

In summary, the novel physical interaction between BLM and MCM revealed in this study is not only essential for the cellular response to DNA damage and replication stress, but is also required in unperturbed cells, most significantly by acting as a negative regulator of DNA replication speed. Specifically, BLM helicase activity appears to be capable of accelerating replication and needs to be tethered to Mcm6 to restrain this capability to the immediate vicinity of the replisome and ensure normal replication speed (Figure 6D). Notably, aberrant acceleration of replication forks beyond a safe limit at which cells become unable to efficiently detect and repair DNA damage was recently suggested to be the mechanism by which PARP inhibitors such as olaparib kill BRCA1-deficient cancer cells (60,79). Similarly, Cdc7 inhibitors, which reduce Mcm2 phosphorylation necessary for initiation of DNA replication (80), can cause aberrant acceleration of DNA replication (65) and are currently in clinical trials for the treatment of metastatic solid tumors. The BLM mutants identified in this study provide powerful tools for elucidating the mechanism by which the BLM/Mcm6 interaction functions as a novel negative regulator of DNA replication speed and for investigating the consequences that inhibition of the interaction will have on the viability of cancer cells as well as on genome stability in normal cells.

## DATA AVAILABILITY

Mass spectrometry proteomics data have been deposited to the ProteomeXchange Consortium (http://proteomecentral.proteomexchange.org) via the PRIDE partner repository (34) with the dataset identifier PXD018823.

## SUPPLEMENTARY DATA

Supplementary Data are available at NAR Online.

## ACKNOWLEDGEMENTS

## FUNDING

## REFERENCES

1. Zeman,M.K. and Cimprich,K.A. (2014) Causes and consequences of replication stress. *Nat. Cell Biol.*, **16**, 2–9.
2. Karow,J.K., Chakraverty,R.K. and Hickson,I.D. (1997) The Bloom's syndrome gene product is a 3′-5′ DNA helicase. *J. Biol. Chem.*, **272**, 30611–30614.
3. Ouyang,K.J., Woo,L.L. and NA,E. (2008) Homologous recombination and maintenance of genome integrity: cancer and aging through the prism of human RecQ helicases. *Mech. Ageing Dev.*, **129**, 425–440.
4. Hickson,I.D. (2003) RecQ helicases: caretakers of the genome. *Nat. Rev. Cancer*, **3**, 169–178.
5. Chaganti,R.S.K., Schonberg,S. and German,J. (1974) A manyfold increase in sister chromatid exchanges in Bloom's syndrome lymphocytes. *Proc. Natl. Acad. Sci. U.S.A.*, **71**, 4508–4512.
6. Ellis,N.A., Groden,J., Ye,T.Z., Straughen,J., Lennon,D.J., Ciocci,S., Proytcheva,M. and German,J. (1995) The Bloom's syndrome gene product is homologous to RecQ helicases. *Cell*, **83**, 655–666.
7. German,J. and Ellis,N.A. (1998) Bloom Syndrome. In: *The genetic basis of human cancer*. McGraw Hill Companies, NY, pp. 301–315.
8. Wu,L. and Hickson,I.D. (2003) The Bloom's syndrome helicase suppresses crossing over during homologous recombination. *Nature*, **426**, 870–874.
9. Daley,J.M., Chiba,T., Xue,X., Niu,H. and Sung,P. (2014) Multifaceted role of the Topo IIIalpha-RMI1-RMI2 complex and DNA2 in the BLM-dependent pathway of DNA break end resection. *Nucleic Acids Res.*, **42**, 11083–11091.
10. Sidorova,J.M., Kehrli,K., Mao,F. and Monnat,R. Jr (2013) Distinct functions of human RECQ helicases WRN and BLM in replication fork recovery and progression after hydroxyurea-induced stalling. *DNA Repair (Amst.)*, **12**, 128–139.
11. Davies,S.L., North,P.S. and Hickson,I.D. (2007) Role for BLM in replication-fork restart and suppression of origin firing after replicative stress. *Nat. Struct. Mol. Biol.*, **14**, 677–679.
12. Davalos,A.R. and Campisi,J. (2003) Bloom syndrome cells undergo p53-dependent apoptosis and delayed assembly of BRCA1 and NBS1 repair complexes at stalled replication forks. *J. Cell Biol.*, **162**, 1197–1209.
13. Franchitto,A. and Pichierri,P. (2002) Bloom's syndrome protein is required for correct relocalization of RAD50/MRE11/NBS1 complex after replication fork arrest. *J. Cell Biol.*, **157**, 19–30.
14. Machwe,A., Xiao,L., Groden,J. and Orren,D.K. (2006) The Werner and Bloom syndrome proteins catalyze regression of a model replication fork. *Biochemistry*, **45**, 13939–13946.
15. Wu,L., Davies,S.L., Levitt,N.C. and Hickson,I.D. (2001) Potential role for the BLM helicase in recombinational repair via a conserved interaction with RAD51. *J. Biol. Chem.*, **276**, 19375–19381.
16. Wyatt,H.D., Sarbajna,S., Matos,J. and West,S.C. (2013) Coordinated actions of SLX1-SLX4 and MUS81-EME1 for Holliday junction resolution in human cells. *Mol. Cell*, **52**, 234–247.
17. Sun,H., Karow,J.K., Hickson,I.D. and Maizels,N. (1998) The Bloom's syndrome helicase unwinds G4 DNA. *J. Biol. Chem.*, **273**, 27587–27592.
18. Popuri,V., Bachrati,C.Z., Muzzolini,L., Mosedale,G., Costantini,S., Giacomini,E., Hickson,I.D. and Vindigni,A. (2008) The human RecQ helicases, BLM and RECQ1, display distinct DNA substrate specificities. *J. Biol. Chem.*, **283**, 17766–17776.
19. Wu,W.Q., Hou,X.M., Li,M., Dou,S.X. and Xi,X.G. (2015) BLM unfolds G-quadruplexes in different structural environments through different mechanisms. *Nucleic Acids Res.*, **43**, 4614–4626.
20. Bochman,M.L., Paeschke,K. and Zakian,V.A. (2012) DNA secondary structures: stability and function of G-quadruplex structures. *Nature reviews. Genetics*, **13**, 770–780.
21. van Wietmarschen,N., Merzouk,S., Halsema,N., Spierings,D.C.J., Guryev,V. and Lansdorp,P.M. (2018) BLM helicase suppresses recombination at G-quadruplex motifs in transcribed genes. *Nat. Commun.*, **9**, 271.
22. Drosopoulos,W.C., Kosiyatrakul,S.T. and Schildkraut,C.L. (2015) BLM helicase facilitates telomere replication during leading strand synthesis of telomeres. *J. Cell Biol.*, **210**, 191–208.
23. Grierson,P.M., Lillard,K., Behbehani,G.K., Combs,K.A., Bhattacharyya,S., Acharya,S. and Groden,J. (2012) BLM helicase facilitates RNA polymerase I-mediated ribosomal RNA transcription. *Hum. Mol. Genet.*, **21**, 1172–1183.
24. Chang,E.Y., Novoa,C.A., Aristizabal,M.J., Coulombe,Y., Segovia,R., Chaturvedi,R., Shen,Y., Keong,C., Tam,A.S., Jones,S.J.M. *et al.* (2017) RECQ-like helicases Sgs1 and BLM regulate R-loop-associated genome instability. *J. Cell Biol.*, **216**, 3991–4005.
25. Kang,S., Kang,M.S., Ryu,E. and Myung,K. (2018) Eukaryotic DNA replication: Orchestrated action of multi-subunit protein complexes. *Mutat. Res.*, **809**, 58–69.
26. Ibarra,A., Schwob,E. and Méndez,J. (2008) Excess MCM proteins protect human cells from replicative stress by licensing backup origins of replication. *Proc. Natl. Acad. Sci. U.S.A.*, **105**, 8956–8961.
27. Cortez,D., Glick,G. and Elledge,S.J. (2004) Minichromosome maintenance proteins are direct targets of the ATM and ATR checkpoint kinases. *PNAS*, **101**, 10078–10083.
28. Chen,Y.H., Jones,M.J., Yin,Y., Crist,S.B., Colnaghi,L., Sims,R.J., Rothenberg,E., Jallepalli,P.V. and Huang,T.T. (2015) ATR-mediated phosphorylation of FANCI regulates dormant origin firing in response to replication stress. *Mol. Cell*, **58**, 323–338.
29. Leman,A.R. and Noguchi,E. (2013) The replication fork: understanding the eukaryotic replication machinery and the challenges to genome duplication. *Genes*, **4**, 1–32.
30. Subramanian,V., Rodemoyer,B., Shastri,V., Rasmussen,L.J., Desler,C. and Schmidt,K.H. (2021) Bloom syndrome DNA helicase deficiency is associated with oxidative stress and mitochondrial network changes. *Sci. Rep.*, **11**, 2157.
31. Xu,X., Rochette,P.J., Feyissa,E.A., Su,T.V. and Liu,Y. (2009) MCM10 mediates RECQ4 association with MCM2-7 helicase complex during DNA replication. *EMBO J.*, **28**, 3005–3014.
32. Rios-Doria,J., Velkova,A., Dapic,V., Galan-Caridad,J.M., Dapic,V., Carvalho,M.A., Melendez,J. and Monteiro,A.N. (2009) Ectopic expression of histone H2AX mutants reveals a role for its post-translational modifications. *Cancer Biol. Ther.*, **8**, 422–434.
33. Cox,J. and Mann,M. (2008) MaxQuant enables high peptide identification rates, individualized p.p.b.-range mass accuracies and proteome-wide protein quantification. *Nat. Biotechnol.*, **26**, 1367–1372.
34. Vizcaino,J.A., Cote,R.G., Csordas,A., Dianes,J.A., Fabregat,A., Foster,J.M., Griss,J., Alpi,E., Birim,M., Contell,J. *et al.* (2013) The PRoteomics IDEntifications (PRIDE) database and associated tools: status in 2013. *Nucleic Acids Res.*, **41**, D1063–D1069.
35. Bussen,W., Raynard,S., Busygina,V., Singh,A.K. and Sung,P. (2007) Holliday junction processing activity of the BLM-Topo IIIalpha-BLAP75 complex. *J. Biol. Chem.*, **282**, 31484–31492.
36. Sakwe,A.M., Nguyen,T., Athanasopoulos,V., Shire,K. and Frappier,L. (2007) Identification and characterization of a novel component of the human minichromosome maintenance complex. *Mol. Cell. Biol.*, **27**, 3044–3055.
37. Ritzi,M., Tillack,K., Gerhardt,J., Ott,E., Humme,S., Kremmer,E., Hammerschmidt,W. and Schepers,A. (2003) Complex protein-DNA dynamics at the latent origin of DNA replication of Epstein-Barr virus. *J. Cell Sci.*, **116**, 3971–3984.
38. Couch,F.B., Bansbach,C.E., Driscoll,R., Luzwick,J.W., Glick,G.G., Betous,R., Carroll,C.M., Jung,S.Y., Qin,J., Cimprich,K.A. *et al.* (2013) ATR phosphorylates SMARCAL1 to prevent replication fork collapse. *Genes Dev.*, **27**, 1610–1623.
39. Wu,L., Davies,S.L., North,P.S., Goulaouic,H., Riou,J.F., Turley,H., Gatter,K.C. and Hickson,I.D. (2000) The Bloom's syndrome gene product interacts with topoisomerase III. *J. Biol. Chem.*, **275**, 9636–9644.
40. Singh,T.R., Ali,A.M., Busygina,V., Raynard,S., Fan,Q., Du,C.H., Andreassen,P.R., Sung,P. and Meetei,A.R. (2008) BLAP18/RMI2, a novel OB-fold-containing protein, is an essential component of the Bloom helicase-double Holliday junction dissolvasome. *Genes Dev.*, **22**, 2856–2868.
41. Bischof,O., Kim,S.H., Irving,J., Beresten,S., Ellis,N.A. and Campisi,J. (2001) Regulation and localization of the Bloom syndrome protein in response to DNA damage. *J. Cell Biol.*, **153**, 367–380.
42. Riera,A., Barbon,M., Noguchi,Y., Reuter,L.M., Schneider,S. and Speck,C. (2017) From structure to mechanism-understanding initiation of DNA replication. *Genes Dev.*, **31**, 1073–1088.
43. Boehm,E.M. and Washington,M.T. (2016) R.I.P. to the PIP: PCNA-binding motif no longer considered specific: PIP motifs and

other related sequences are not distinct entities and can bind multiple proteins involved in genome maintenance. *Bioessays*, **38**, 1117–1122.

44. Wei,Z., Liu,C., Wu,X., Xu,N., Zhou,B., Liang,C. and Zhu,G. (2010) Characterization and structure determination of the Cdt1 binding domain of human minichromosome maintenance (Mcm) 6. *J. Biol. Chem.*, **285**, 12469–12473.

45. Fernandez-Cid,A., Riera,A., Tognetti,S., Herrera,M.C., Samel,S., Evrin,C., Winkler,C., Gardenal,E., Uhle,S. and Speck,C. (2013) An ORC/Cdc6/MCM2-7 complex is formed in a multistep reaction to serve as a platform for MCM double-hexamer assembly. *Mol. Cell*, **50**, 577–588.

46. Zhang,J., Yu,L., Wu,X., Zou,L., Sou,K.K., Wei,Z., Cheng,X., Zhu,G. and Liang,C. (2010) The interacting domains of hCdt1 and hMcm6 involved in the chromatin loading of the MCM complex in human cells. *Cell Cycle*, **9**, 4848–4857.

47. Hosoi,A., Sakairi,T. and Yukio,I. (2015) Binding of MCM-interacting proteins to ATP-binding site in MCM6. *Res. Rep. Biol.*, **2016**, 31–40.

48. Sun,L., Huang,Y., Edwards,R.A., Yang,S., Blackford,A.N., Niedzwiedz,W. and Glover,J.N.M. (2017) Structural Insight into BLM Recognition by TopBP1. *Structure*, **25**, 1582–1588.

49. Blackford,A.N., Nieminuszczy,J., Schwab,R.A., Galanty,Y., Jackson,S.P. and Niedzwiedz,W. (2015) TopBP1 interacts with BLM to maintain genome stability but is dispensable for preventing BLM degradation. *Mol. Cell*, **57**, 1133–1141.

50. Frigola,J., He,J., Kinkelin,K., Pye,V.E., Renault,L., Douglas,M.E., Remus,D., Cherepanov,P., Costa,A. and Diffley,J.F.X. (2017) Cdt1 stabilizes an open MCM ring for helicase loading. *Nat. Commun.*, **8**, 15720.

51. Looke,M., Maloney,M.F. and Bell,S.P. (2017) Mcm10 regulates DNA replication elongation by stimulating the CMG replicative helicase. *Genes Dev.*, **31**, 291–305.

52. Davies,S.L., North,P.S., Dart,A., Lakin,N.D. and Hickson,I.D. (2004) Phosphorylation of the Bloom's syndrome helicase and its role in recovery from S-phase arrest. *Mol. Cell. Biol.*, **24**, 1279–1291.

53. Shastri,V.M. and Schmidt,K.H. (2016) Cellular defects caused by hypomorphic variants of the Bloom syndrome helicase gene BLM. *Mol. Genet. Genomic Med.*, **4**, 106–119.

54. Budhathoki,J.B., Ray,S., Urban,V., Janscak,P., Yodh,J.G. and Balci,H. (2014) RecQ-core of BLM unfolds telomeric G-quadruplex in the absence of ATP. *Nucleic Acids Res.*, **42**, 11528–11545.

55. Mohaghegh,P., Karow,J.K., Brosh,R.M. Jr, Bohr,V.A. and Hickson,I.D. (2001) The Bloom's and Werner's syndrome proteins are DNA structure-specific helicases. *Nucleic Acids Res.*, **29**, 2843–2849.

56. London,T.B., Barber,L.J., Mosedale,G., Kelly,G.P., Balasubramanian,S., Hickson,I.D., Boulton,S.J. and Hiom,K. (2008) FANCJ is a structure-specific DNA helicase associated with the maintenance of genomic G/C tracts. *J. Biol. Chem.*, **283**, 36132–36139.

57. Rodriguez,R., Miller,K.M., Forment,J.V., Bradshaw,C.R., Nikan,M., Britton,S., Oelschlaegel,T., Xhemalce,B., Balasubramanian,S. and Jackson,S.P. (2012) Small-molecule-induced DNA damage identifies alternative DNA structures in human genes. *Nat. Chem. Biol.*, **8**, 301–310.

58. Hand,R. and German,J. (1975) A retarded rate of DNA chain growth in Bloom's syndrome. *Proc. Natl. Acad. Sci. U.S.A.*, **72**, 758–762.

59. Rao,V.A., Conti,C., Guirouilh-Barbat,J., Nakamura,A., Miao,Z.H., Davies,S.L., Sacca,B., Hickson,I.D., Bensimon,A. and Pommier,Y. (2007) Endogenous gamma-H2AX-ATM-Chk2 checkpoint activation in Bloom's syndrome helicase deficient cells is related to DNA replication arrested forks. *Mol. Cancer Res.: MCR*, **5**, 713–724.

60. Maya-Mendoza,A., Moudry,P., Merchut-Maya,J.M., Lee,M., Strauss,R. and Bartek,J. (2018) High speed of fork progression induces DNA replication stress and genomic instability. *Nature*, **559**, 279–284.

61. Nieminuszczy,J., Schwab,R.A. and Niedzwiedz,W. (2016) The DNA fibre technique - tracking helicases at work. *Methods*, **108**, 92–98.

62. Chaudhury,I., Sareen,A., Raghunandan,M. and Sobeck,A. (2013) FANCD2 regulates BLM complex functions independently of FANCI to promote replication fork recovery. *Nucleic Acids Res.*, **41**, 6444–6459.

63. Machwe,A., Karale,R., Xu,X., Liu,Y. and Orren,D.K. (2011) The Werner and Bloom syndrome proteins help resolve replication blockage by converting (regressed) holliday junctions to functional replication forks. *Biochemistry*, **50**, 6774–6788.

64. Zhong,Y., Nellimoottil,T., Peace,J.M., Knott,S.R., Villwock,S.K., Yee,J.M., Jancuska,J.M., Rege,S., Tecklenburg,M., Sclafani,R.A. *et al.* (2013) The level of origin firing inversely affects the rate of replication fork progression. *J. Cell Biol.*, **201**, 373–383.

65. Rodriguez-Acebes,S., Mouron,S. and Mendez,J. (2018) Uncoupling fork speed and origin activity to identify the primary cause of replicative stress phenotypes. *J. Biol. Chem.*, **293**, 12855–12861.

66. Takahashi,T.S., Wigley,D.B. and Walter,J.C. (2005) Pumps, paradoxes and ploughshares: mechanism of the MCM2-7 DNA helicase. *Trends Biochem. Sci.*, **30**, 437–444.

67. Sangrithi,M.N., Bernal,J.A., Madine,M., Philpott,A., Lee,J., Dunphy,W.G. and Venkitaraman,A.R. (2005) Initiation of DNA replication requires the RECQL4 protein mutated in Rothmund-Thomson syndrome. *Cell*, **121**, 887–898.

68. Singh,D.K., Popuri,V., Kulikowicz,T., Shevelev,I., Ghosh,A.K., Ramamoorthy,M., Rossi,M.L., Janscak,P., Croteau,D.L. and Bohr,V.A. (2012) The human RecQ helicases BLM and RECQL4 cooperate to preserve genome stability. *Nucleic Acids Res.*, **40**, 6632–6648.

69. Drissi,R., Dubois,M.L., Douziech,M. and Boisvert,F.M. (2015) Quantitative proteomics reveals dynamic interactions of the minichromosome maintenance complex (MCM) in the cellular response to etoposide induced DNA damage. *Mol. Cell. Proteomics*, **14**, 2002–2013.

70. Powell,S.K., MacAlpine,H.K., Prinz,J.A., Li,Y., Belsky,J.A. and MacAlpine,D.M. (2015) Dynamic loading and redistribution of the Mcm2-7 helicase complex through the cell cycle. *EMBO J.*, **34**, 531–543.

71. Arias,E.E. and Walter,J.C. (2006) PCNA functions as a molecular platform to trigger Cdt1 destruction and prevent re-replication. *Nat. Cell Biol.*, **8**, 84–90.

72. Nishitani,H., Sugimoto,N., Roukos,V., Nakanishi,Y., Saijo,M., Obuse,C., Tsurimoto,T., Nakayama,K.I., Nakayama,K., Fujita,M. *et al.* (2006) Two E3 ubiquitin ligases, SCF-Skp2 and DDB1-Cul4, target human Cdt1 for proteolysis. *EMBO J.*, **25**, 1126–1136.

73. Jin,J., Arias,E.E., Chen,J., Harper,J.W. and Walter,J.C. (2006) A family of diverse Cul4-Ddb1-interacting proteins includes Cdt2, which is required for S phase destruction of the replication factor Cdt1. *Mol. Cell*, **23**, 709–721.

74. Hu,P., Beresten,S.F., van Brabant,A.J., Ye,T.Z., Pandolfi,P.P., Johnson,F.B., Guarente,L. and Ellis,N.A. (2001) Evidence for BLM and Topoisomerase IIIalpha interaction in genomic stability. *Hum. Mol. Genet.*, **10**, 1287–1298.

75. Garkavtsev,I.V., Kley,N., Grigorian,I.A. and Gudkov,A.V. (2001) The Bloom syndrome protein interacts and cooperates with p53 in regulation of transcription and cell growth control. *Oncogene*, **20**, 8276–8280.

76. Zhu,J., Zhu,S., Guzzo,C.M., Ellis,N.A., Sung,K.S., Choi,C.Y. and Matunis,M.J. (2008) Small ubiquitin-related modifier (SUMO) binding determines substrate recognition and paralog-selective SUMO modification. *J. Biol. Chem.*, **283**, 29405–29415.

77. Song,J., Durrin,L.K., Wilkinson,T.A., Krontiris,T.G. and Chen,Y. (2004) Identification of a SUMO-binding motif that recognizes SUMO-modified proteins. *Proc. Natl. Acad. Sci. U.S.A.*, **101**, 14373–14378.

78. Wei,L. and Zhao,X. (2016) A new MCM modification cycle regulates DNA replication initiation. *Nat. Struct. Mol. Biol.*, **23**, 209–216.

79. Quinet,A. and Vindigni,A. (2018) Superfast DNA replication causes damage in cancer cells. *Nature*, **559**, 186–187.

80. Jiang,W., McDonald,D., Hope,T.J. and Hunter,T. (1999) Mammalian Cdc7-Dbf4 protein kinase complex is essential for initiation of DNA replication. *EMBO J.*, **18**, 5703–5713.